Letter

Lattice QCD constraints on the critical point from an improved precision equation of state

Szabolcs Borsányi,[1] Zoltán Fodor,[2,3,1,4,5] Jana N. Guenther,[1] Paolo Parotto,[6] Attila Pásztor,[4] Claudia Ratti,[7] Volodymyr Vovchenko,[7] and Chik Him Wong[1]

[1]*University of Wuppertal, Department of Physics, Wuppertal D-42119, Germany*
[2]*Pennsylvania State University, Department of Physics, State College, Pennsylvania 16801, USA*
[3]*Pennsylvania State University, Institute for Computational and Data Sciences, State College, Pennsylvania 16801, USA*
[4]*Institute for Theoretical Physics, ELTE Eötvös Loránd University, Pázmány Péter sétány 1/A, H-1117 Budapest, Hungary*
[5]*Jülich Supercomputing Centre, Forschungszentrum Jülich, D-52425 Jülich, Germany*
[6]*Dipartimento di Fisica, Università di Torino and INFN Torino, Via Pietro Giuria 1, I-10125 Torino, Italy*
[7]*Department of Physics, University of Houston, Houston, Texas 77204, USA*

(Received 10 March 2025; accepted 4 November 2025; published 17 December 2025)

In this paper we employ lattice simulations to search for the critical point of QCD. We search for the onset of a first-order QCD transition on the phase diagram by following contours of constant entropy density from imaginary to real chemical potentials under conditions of strangeness neutrality. We scan the phase diagram and investigate whether these contours meet to determine the probability that the critical point is located in a certain region on the $T - \mu_B$ plane. To achieve this we introduce a new, continuum extrapolated equation of state at zero density with improved precision using lattices with $N_\tau = 8, 10, 12, 16$ time slices, and supplement it with new data at imaginary chemical potential. The current precision allows us to exclude, at the 2σ level, the existence of a critical point at $\mu_B < 450$ MeV.

DOI: 10.1103/rj6r-dmg9

Introduction. The study of the phase diagram of QCD is an extremely active field of research, which encompasses conditions ranging from high energy heavy ion collisions to the mergers of neutron stars. The major tool for *ab initio* investigations of QCD thermodynamics are lattice simulations, which have shown that, at vanishing density, the transition separating the hadronic phase from the quark gluon plasma (QGP) is a broad crossover [1] located at around $T = 155$–160 MeV [2,3].

At finite chemical potential μ_B, based on results from several effective approaches to QCD, it is conjectured that the crossover transition turns into a first-order line at a critical endpoint (see e.g., [4,5]). Lattice QCD at finite density suffers from a complex action problem, which renders simulations extremely costly. Several indirect approaches have been devised to circumvent this issue, most notably Taylor expansion around $\mu_B = 0$ [2,6–14], analytic continuation from imaginary chemical potential [3,12,15–25] and reweighting techniques [26–37]. Results from these methods have been obtained for different quantities, like the equation of state, fluctuations of conserved charges or the QCD transition line, up to chemical potentials as large as $\mu_B \simeq 3.5T$, though no sign of criticality has been observed. Notable exceptions are attempts to extract the position of the corresponding Lee-Yang edge singularity from lattice data [14,38–40].

The quest for the QCD critical point was one of the main motivations behind the extensive Beam Energy Scan program at the Relativistic Heavy Ion Collider, from which final results will come in the near future. Although direct experimental evidence for the existence of a critical point is still missing, both the BES-I [41,42] and BES-II results [43] on net-proton cumulants indicate deviations from noncritical baselines [44,45] at the lowest energies, which might not be explainable without critical effects. At the moment, the uncertainties are still sizable, but more precise data and analysis in the future might clarify the issue.

Several recent predictions for the location of the critical point have been obtained via functional methods [46–51], holography [52–54] and the analysis of experimental data [55–58]. Many (but not all) of these predictions based on different approaches cluster in a rather small region on the QCD phase diagram. However, the systematic uncertainty

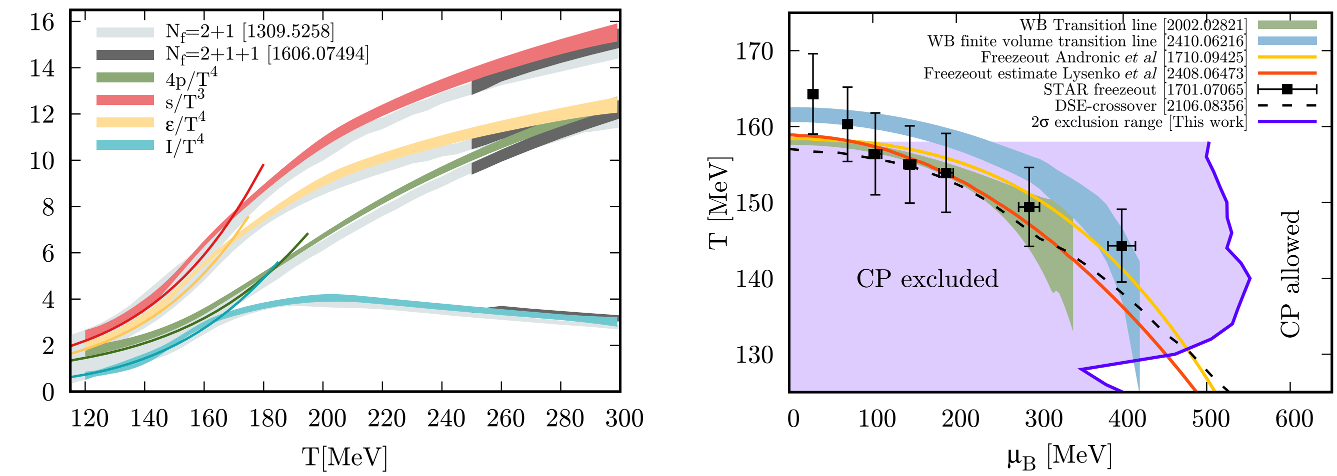

FIG. 1. Left: pressure (green), entropy (red), energy density (yellow) and trace anomaly (cyan) as functions of the temperature. The light and dark gray bands show our previous results from Refs. [60,66], respectively, while the curves at low temperature are the Hadron Resonance Gas (HRG) model results. Right: The QCD phase diagram in the $T - \mu_B$ plane with the 2σ exclusion range obtained in this work. We also show the chiral transition line from the continuum extrapolated lattice simulations in a large volume [3], as well as a recent result in a smaller system without continuum extrapolation [67] and a prediction based on Dyson-Schwinger equations [50]. Besides the STAR result for chemical freeze-out parameters for collision energies $\sqrt{s} = 200 - 7.7$ GeV [63] and its parametrization [64], we add a recent lower bound estimate based on a fixed energy/particle number ratio within the HRG framework [65].

of these approaches is hard to estimate. Hence, a method with controlled systematics is highly desirable.

In Ref. [59] a novel method, based solely on lattice results, was proposed to estimate the location of the critical point by studying contours of constant entropy density on the QCD phase diagram. The idea is to employ the entropy contours to search for the onset of a first-order regime; if different contours meet somewhere in the phase diagram, it means that the entropy has become multivalued, hence the transition has turned first order. By determining where the first-order regime is reached, the location of the critical point can be estimated. In Ref. [59], the entropy contours were constructed based on existing lattice results at vanishing chemical potential for the entropy density [60] and second order baryon susceptibility [24].

In this work, we generalize this method in more than one way. To reach the necessary precision to bear predictive power, we perform a new computation of the equation of state of QCD at zero density, with significantly reduced uncertainties compared to existing results. Instead of extracting the constant entropy contours from $\mu_B = 0$ data, we extrapolate them from imaginary μ_B. In addition, we increase the statistics of data sets at the three highest imaginary chemical potentials on the finest lattice in comparison to our earlier work [25]. While the extrapolation in Ref. [59] was done at order $\mathcal{O}(\mu_B^2)$, here we allow for leading corrections to the linear μ_B^2 dependence. We use the actual statistical correlations between variables and also consider additional sources of systematic errors in the analysis. Besides, the results presented in Ref. [59] were obtained for zero strangeness chemical potential, while here we enforce strangeness neutrality.

One of the advantages of the entropy contours method is that it does not rely on detecting criticality directly. In lattice simulations, this means that it is not necessary to employ large volumes to accommodate a diverging correlation length. Throughout this work, we employ lattices with an aspect ratio $LT = 4$. We showed in Ref. [61] that such a physical volume is sufficient to essentially eliminate finite volume effects on the QCD transition temperature. We also showed that volume effects on the μ_B dependence of the QCD transition, akin to the entropy contours we employ in this work, are well under control.

There are two main results in this paper. We present an update of the zero-density equation of state (see tabulated data in the Supplemental Material [62]). We also determine an exclusion probability for the existence of a critical point as a function of the chemical potential. We show both results in Fig. 1. We obtain our final result by combining our excluded region with the available information on the chemical freeze-out line [63–65]. To be conservative, we choose the curve in Ref. [65], which was estimated as a lower bound for the freeze-out temperature, and thus, also for T_c. We find that, at the 2σ level, we can exclude the existence of a critical point below $\mu_B^{2\sigma} = 450$ MeV.

In the following, we discuss the ingredients that have led us to this finding. We first introduce the update to the zero-density equation of state [60] at $\mu_B = 0$ in the temperature range $T = 120$–300 MeV. We extend the entropy function to imaginary μ_B by continuum extrapolating the imaginary baryon density and its temperature derivative at these μ_B, maintaining strangeness neutrality. Finally, the contours of constant entropy are extrapolated to $\mu_B > 0$, and we calculate the probability for the entropy to be multivalued at each point on the phase diagram.

Equation of state at $\mu_B = 0$. Throughout the analysis, we employ our 4stout staggered action with $N_f = 2 + 1 + 1$ quarks at physical quark masses. Thus, we compute the QCD pressure including the dynamical contribution of the charm quark. In Ref. [66] we already computed the equation of state with this lattice action at high temperatures, now we complement this to the transition region. Here the charm quark plays an insignificant role except for high temperatures, $T \gtrsim 250$ MeV. Methodically, we proceed as in Ref. [60], where the $2 + 1$ flavor equation of state was computed earlier by us.

To determine the equation of state at vanishing chemical potential, we employ the integral method of Ref. [68], whereby the pressure is obtained through the integration of the trace anomaly,

$$\frac{p(T)}{T^4} = \frac{p(T_0)}{T_0^4} + \int_{T_0}^{T} \frac{dT'}{T'} \frac{I(T')}{T'^4}, \tag{1}$$

where $\frac{p(T_0)}{T_0^4}$ is an integration constant.

The integration constant and the trace anomaly are addressed separately with designated lattice runs, both are extrapolated to the continuum limit. We do not use model-dependent input (such as hadron resonance gas) to fix the integration constant, or to constrain the continuum limit.

Equation (1) is a multidimensional line integral in the space of the bare parameters of the action—the gauge coupling $\beta = 6/g^2$ and the fermion masses m_f—along the line of constant physics $m_f(\beta)$. The bare parameters of this discretization have been documented in Ref. [69]. Throughout this work, we use physical quark masses on $N_t = 8$, 10, 12, 16 lattices.

The trace anomaly can be written as

$$\frac{I(T)}{T^4} = -T N_\tau^4 \frac{d\beta}{dT} \left(\langle -s_G \rangle + \sum_f \frac{dm_f}{d\beta} \langle \bar{\psi}_f \psi_f \rangle \right), \tag{2}$$

where $d\beta/dT$ is given by the scale setting and the $dm_f/d\beta$ are given by the line of constant physics. The expectation values $\langle -s_G \rangle$ and $\langle \bar{\psi}_f \psi_f \rangle$ are the gauge action and the chiral condensates, respectively. Both quantities require additive renormalization, which is carried out by subtracting the vacuum contribution at the same bare parameters,

$$\langle -s_G \rangle = \langle -s_G \rangle_T - \langle -s_G \rangle_0, \tag{3}$$

$$\langle \bar{\psi}_f \psi_f \rangle = \langle \bar{\psi}_f \psi_f \rangle_T - \langle \bar{\psi}_f \psi_f \rangle_0. \tag{4}$$

We performed a large number of zero-temperature simulations to reduce the noise on the vacuum term in Eq. (3), which is responsible for much of the error on the trace anomaly itself [70]. We determine the trace anomaly in the range $T = 120$–300 MeV by combining a linear continuum limit in $1/N_\tau^2$ with a spline fit in the temperature. Details on the statistics and the fit procedure can be found in the Supplemental Material [62]. The continuum extrapolated trace anomaly is shown in Fig. 2, together with the results on individual lattices.

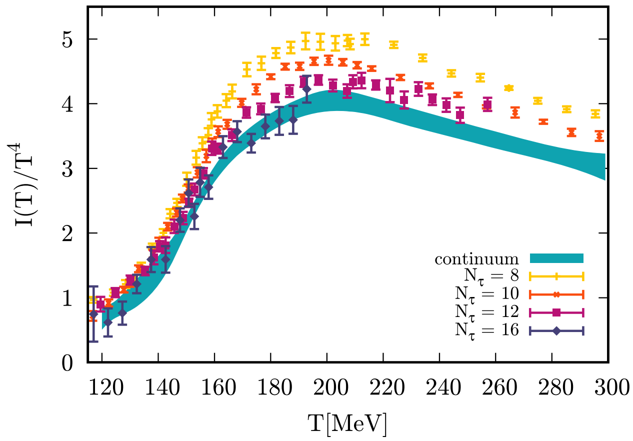

FIG. 2. Trace anomaly in the continuum (cyan band), as well as at finite N_τ (colored points).

The integration constant in Eq. (1) is determined in a similar way, by integrating the chiral condensate in the fermion masses from infinity, where the pressure vanishes, down to the physical values. In practice, it is sufficient to start from the mass of the charm quark m_c, integrate the three-flavor theory down to the strange quark mass m_s, then integrate the two-flavor theory down to the light quark mass m_l,

$$\frac{p(T_0)}{T_0^4} = \int_{m_s}^{m_l} dm_2 \langle \bar{\psi}\psi \rangle_2(m_2) + \int_{\infty}^{m_s} dm_3 \langle \bar{\psi}\psi \rangle_3(m_3). \tag{5}$$

Here, the subscripts 2,3 refer to the $N_f = 2$, 3 flavor theories, and the chiral condensates are the renormalized ones. In this work we choose to calculate this constant at $T_0 = 185$ MeV, to minimize the uncertainty on the equation of state in the transition region.

For the continuum extrapolation of $p(T_0)/T_0^4$ we include $N_\tau = 10$, 12, 16 lattices. Several sources of systematic uncertainties are considered, for a total of 32 analyses, which are then combined with the histogram method introduced in Ref. [71]. The final result is

$$\frac{p(T_0 = 185\ \text{MeV})}{T_0^4} = 1.371(28), \tag{6}$$

where the quoted error includes both statistical and systematic uncertainties. The precision we reach is approximately a 2× improvement over our previous result [60].

Details on the extrapolation and the systematic analyses can be found in the Supplemental Material.

With Eq. (1) we can now determine the pressure, and from it the other thermodynamic quantities. Trace anomaly, pressure, entropy and energy density are shown in the left panel of Fig. 1 as colored bands, together with our previous results from Refs. [60,66], shown as gray bands for comparison. The improved precision in both terms of Eq. (1) results in a substantial improvement for the precision of all quantities, especially near the transition region. At high temperatures our data agree with Ref. [66] better than with Ref. [60], as the latter is a $N_f = 2 + 1$ result. A minor tension remains between our new result and Ref. [66] in the pressure, which is likely due to the new determination of the integration constant in Eq. (1). In Ref. [66] this integration constant was fixed to be the $N_f = 2 + 1$ result of Ref. [60] at $T = 250$ MeV.

Entropy contours. In this work we construct and follow contours of constant entropy density from imaginary to real baryon chemical potential. These contours are defined at vanishing strangeness density and zero electric charge chemical potential. At finite (real or imaginary) μ_B, the entropy density can be written as

$$s(T, \mu_B) = s(T, \mu_B = 0) + \int_0^{\mu_B} d\mu'_B \frac{\partial n_B(T, \mu'_B)}{\partial T}, \quad (7)$$

where the first term comes from the continuum extrapolated equation of state discussed in the previous section, and $n_B(T, \mu_B)$ is the baryon density. We construct a continuum extrapolation of $n_B(T, \mu_B)$ for imaginary values of the chemical potential μ_B by employing simulations at imaginary chemical potentials on lattices with $N_\tau = 10$, 12, and 16 time slices. We perform a combined fit in the temperature T, the baryochemical potential μ_B and the lattice spacing $1/N_\tau^2$. Details on the fit and the systematic analyses can be found in the Supplemental Material.

From the continuum extrapolated baryon density we construct the entropy density at imaginary chemical potential using Eq. (7). In order to construct the contours, we proceed as follows. For each temperature T_0, we first calculate the corresponding value $s(T_0)$ of the entropy at $\mu_B = 0$. For each chemical potential, we then determine the temperature $T_s(\mu_B, T_0)$ at which the entropy has the desired value $s(T_0)$. The function $T_s(\mu_B, T_0)$ then yields the contour stemming from T_0. By repeating the procedure for several values of T_0, we obtain the contours shown as points in Fig. 3 for $\mu_B^2 < 0$. We observe that the dependence of $T_s(T_0, \mu_B)$ on μ_B^2 is remarkably linear to a high precision.

We do not expect entropy contours to deviate significantly from the functional forms we have used, even in the presence of a first-order transition, as the entropy itself must obey thermodynamic inequalities that limit its T and μ_B derivatives.

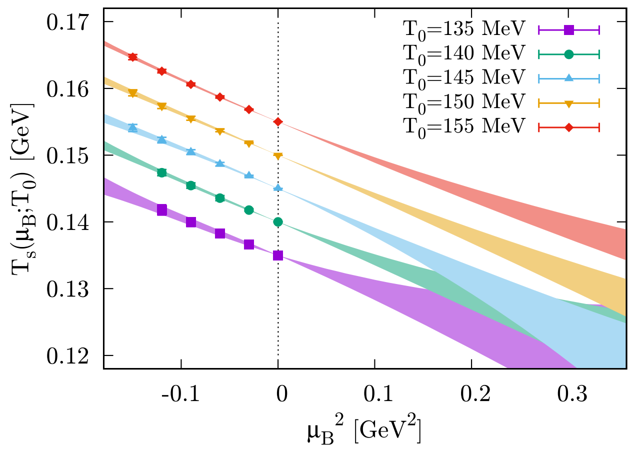

FIG. 3. Contours of constant (dimensionful) entropy density as fitted rational functions on continuum extrapolated lattice data. Each contour is labeled by its crossing point at $\mu_B = 0$: T_0. Note that the extrapolation is defined in the dimensionful μ_B^2 (see also [59]), not μ_B/T.

In order to account for deviations from an exact linear behavior, we consider an extrapolation to real chemical potential based on a rational *Ansatz* as well as a parabolic *Ansatz*,

$$T_s(\mu_B^2, T_0) = \frac{T_0 + a\mu_B^2}{1 + b\mu_B^2}, \quad (8)$$

$$T_s(\mu_B^2, T_0) = T_0 + a\mu_B^2 + b\mu_B^4, \quad (9)$$

that we combine to obtain our final results. We performed Kolmogorov-Smirnov tests on our sets of analyses with both functional forms, and found that both are at risk of overfitting. For this reason, we do not consider functional forms with more parameters. We show the results obtained with the rational *Ansatz* as bands in Fig. 3.

In order to determine the onset of a first-order transition regime on the phase diagram, we now study the contours $T_s(\mu_B^2, T_0)$ for different, fixed values of μ_B. Because the entropy is a monotonic function of the temperature in the absence of a discontinuity, the curve $T_s(\mu_B^2, T_0)$ will be, at fixed μ_B, monotonic as well. However, if and when the entropy develops a discontinuity, there will be a regime where the derivative $(\partial T_s/\partial T_0)_{\mu_B}$ drops below zero, while being exactly zero at the critical point. We can see a pattern similar to the expected one in Fig. 4, where $T_s(\mu_B^2, T_0)$ is shown for two values of μ_B in the case of our rational *Ansatz*. At large chemical potentials data are consistent with a zero or negative derivative within some level of confidence (e.g., $\mu_B = 600$ MeV in Fig. 4).

We identify this confidence level for each $T - \mu_B$ pair in the phase diagram. First, we solve $T = T_s(\mu_B^2, T_0)$ for T_0, and then evaluate $(\partial T_s/\partial T_0)_{\mu_B}$ at that value. For a broad range of parameters, this is at least one or two σ larger than

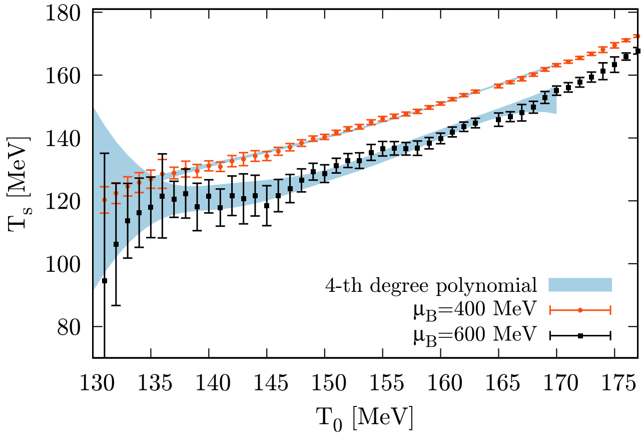

FIG. 4. The value of $T_s(\mu_B^2, T_0)$ for two fixed values of the baryochemical potential. These curves develop a negative derivative in the first-order regime, and an exactly vanishing derivative at the critical point.

zero, indicating that at the given $T - \mu_B$ position, the entropy is not multivalued to the given level of confidence.

We exemplify this in the top panel of Fig. 5. The two curves represent two horizontal stripes in the phase diagram, where this analysis was carried out. The plot shows the levels that would belong to 1σ and 2σ around the central value, if the distribution was Gaussian. We translate this to a confidence level in the bottom panel. There we also show the probability of having a negative slope of $T_s(T_0)$ along two versions of the chemical freeze-out line [64,65] and a prediction of the crossover line [50] in the phase diagram.

The data in Fig. 5 already refer to the full systematic analysis. In particular, we performed 16 different continuum extrapolations to arrive at the entropy at imaginary μ_B, extrapolated to $\mu_B > 0$ with our two *Ansätze*, and each resulting T_s function was interpolated in 12 different ways. Though each of the $12 \cdot 2 \cdot 16 = 384$ such analyses provides a Gaussian statistical error, once their respective cumulative distribution function is averaged, the result is non-Gaussian. Restricting the analysis to either of the *Ansätze* would leave unchanged the conclusions of our paper. The main result in Fig. 1 shows the chemical potential for a set of fixed temperatures where the confidence level reaches 0.02275 for 2σ. At the 2σ confidence level the lower bound is $\mu_B^{2\sigma} = 450$ MeV.

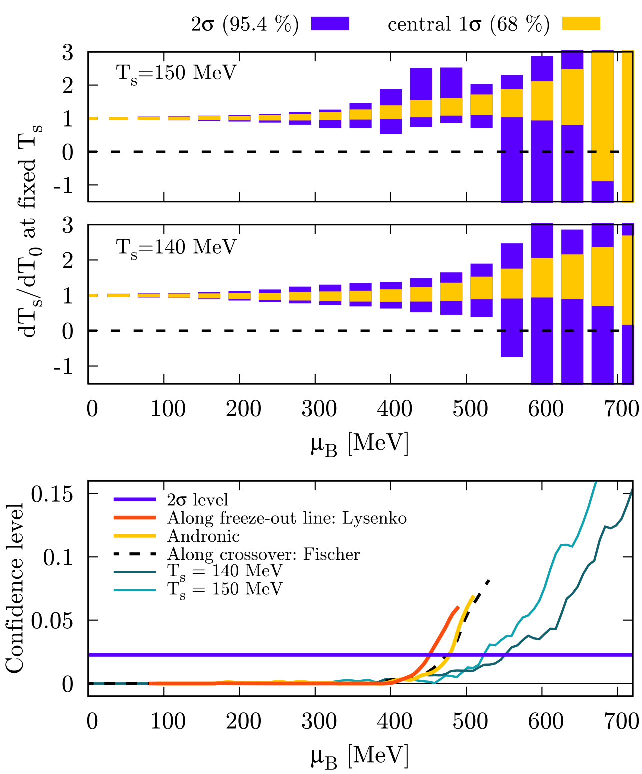

FIG. 5. Top: The derivative of the $T_s(T_0)$ curve at fixed chemical potential as a function of T_0 (see Fig. 4). This quantity is positive for a crossover, negative for a first-order transition and zero at the critical point. Bottom: The confidence level for the $(\partial T_s/\partial T_0)_{\mu_B} < 0$ hypothesis for two fixed values of T_s and along the predicted crossover line of Ref. [50]. We also show the confidence levels along the two freeze-out lines in Fig. 1.

Conclusions. We presented an update of the QCD equation of state at $\mu_B = 0$ with improved precision in comparison to our previous result [60]. This result was obtained with the $(2+1+1$ flavor) 4stout staggered action up to a resolution of $N_\tau = 16$ to perform a continuum extrapolation.

This allowed us to calculate contours of constant entropy on the QCD phase diagram in the $T - \mu_B$ plane, by analytic continuation from purely imaginary chemical potentials using continuum extrapolated lattice QCD simulations in a large volume: $LT = 4$ in temperature units. Unlike previous estimates based on lattice simulations, we show results on the phenomenologically relevant strangeness neutral line. The contours of constant entropy in principle allow one to locate the spinodal region, and thus the onset of a first-order transition at the coveted critical endpoint. While some of the considered analyses indeed show a critical endpoint, we have found that after taking into account all systematic and statistical uncertainties, the location of the critical endpoint cannot be unambiguously bracketed. This also means that our analysis does not provide a clear proof of the existence of such a critical endpoint. However—for the first time in the literature—we are able to give reliable lower bounds on the critical endpoint location in continuum QCD.

Supplementing the analysis with the known heavy-ion chemical freeze-out line (Fig. 1), we can exclude the existence of the critical point, at the 2σ level, below $\mu_B^{2\sigma} = 450$ MeV. Our results for the critical endpoint are consistent with the conclusions from an analysis of the Polyakov loop in a small physical volume in Ref. [67], where a broadening of the crossover transition was observed at $\mu_B \lesssim 400$ MeV.

From chiral effective models one expects the transition temperature in the chiral limit at zero density to be an upper bound for the critical point at finite density [72]. The O(4) critical temperature in the chiral limit was recently calculated to be $T_\chi \sim 133$ MeV [73,74]. Translating our lower bound on the critical chemical potential to an upper bound in temperature, our finding is consistent with the above expectation.

Acknowledgments. This work is supported by the MKW NRW under the funding code NW21-024-A. Further funding was received from the DFG under the Project No. 496127839. This work was also supported by the Hungarian National Research, Development and Innovation Office, NKFIH Grant No. KKP126769. This work was also supported by the NKFIH excellence Grant No. TKP2021_NKTA_64. This work is also supported by the Hungarian National Research, Development and Innovation Office under Project No. FK 147164. This material is also based upon work supported by the National Science Foundation under Grants No. PHY-2208724, and No. PHY-2116686, and within the framework of the MUSES Collaboration, under Grant No. No. OAC-2103680. This material is also based upon work supported by the U.S. Department of Energy, Office of Science, Office of Nuclear Physics, under Awards No. DE-SC0022023, No. DE-SC0025025, and No. DE-SC0026065, as well as by the National Aeronautics and Space Agency (NASA) under Award No. 80NSSC24K0767. The authors gratefully acknowledge the Gauss Centre for Supercomputing e.V. [75] for funding this project by providing computing time on the GCS Supercomputer HAWK at HLRS, Stuttgart. An award of computer time was provided by the INCITE program. This research used resources of the Argonne Leadership Computing Facility, which is a DOE Office of Science User Facility supported under Contract No. DE-AC02-06CH11357.

Data availability. The data that support the findings of this article are openly available [76], embargo periods may apply.

[1] Y. Aoki, G. Endrodi, Z. Fodor, S. D. Katz, and K. K. Szabo, The order of the quantum chromodynamics transition predicted by the standard model of particle physics, Nature (London) **443**, 675 (2006).

[2] A. Bazavov *et al.* (HotQCD Collaboration), Chiral crossover in QCD at zero and non-zero chemical potentials, Phys. Lett. B **795**, 15 (2019).

[3] S. Borsanyi, Z. Fodor, J. N. Guenther, R. Kara, S. D. Katz, P. Parotto, A. Pasztor, C. Ratti, and K. K. Szabo, QCD crossover at finite chemical potential from lattice simulations, Phys. Rev. Lett. **125**, 052001 (2020).

[4] A. Bzdak, S. Esumi, V. Koch, J. Liao, M. Stephanov, and N. Xu, Mapping the phases of quantum chromodynamics with beam energy scan, Phys. Rep. **853**, 1 (2020).

[5] L. Du, A. Sorensen, and M. Stephanov, The QCD phase diagram and beam energy scan physics: A theory overview, Int. J. Mod. Phys. E **33**, 2430008 (2024).

[6] C. R. Allton, S. Ejiri, S. J. Hands, O. Kaczmarek, F. Karsch, E. Laermann, and C. Schmidt, The equation of state for two flavor QCD at nonzero chemical potential, Phys. Rev. D **68**, 014507 (2003).

[7] C. R. Allton, M. Doring, S. Ejiri, S. J. Hands, O. Kaczmarek, F. Karsch, E. Laermann, and K. Redlich, Thermodynamics of two flavor QCD to sixth order in quark chemical potential, Phys. Rev. D **71**, 054508 (2005).

[8] O. Kaczmarek, F. Karsch, E. Laermann, C. Miao, S. Mukherjee, P. Petreczky, C. Schmidt, W. Soeldner, and W. Unger, Phase boundary for the chiral transition in $(2+1)$ -flavor QCD at small values of the chemical potential, Phys. Rev. D **83**, 014504 (2011).

[9] G. Endrodi, Z. Fodor, S. D. Katz, and K. K. Szabo, The QCD phase diagram at nonzero quark density, J. High Energy Phys. 04 (2011) 001.

[10] S. Borsanyi, G. Endrodi, Z. Fodor, S. D. Katz, S. Krieg, C. Ratti, and K. K. Szabo, QCD equation of state at nonzero chemical potential: Continuum results with physical quark masses at order mu^2, J. High Energy Phys. 08 (2012) 053.

[11] A. Bazavov *et al.*, The QCD equation of state to $\mathcal{O}(\mu_B^6)$ from lattice QCD, Phys. Rev. D **95**, 054504 (2017).

[12] C. Bonati, M. D'Elia, F. Negro, F. Sanfilippo, and K. Zambello, Curvature of the pseudocritical line in QCD: Taylor expansion matches analytic continuation, Phys. Rev. D **98**, 054510 (2018).

[13] A. Bazavov *et al.* (HotQCD Collaboration), Chiral crossover in QCD at zero and non-zero chemical potentials, Phys. Lett. B **795**, 15 (2019).

[14] D. Bollweg, J. Goswami, O. Kaczmarek, F. Karsch, S. Mukherjee, P. Petreczky, C. Schmidt, and P. Scior (HotQCD Collaboration), Taylor expansions and Padé approximants for cumulants of conserved charge fluctuations at nonvanishing chemical potentials, Phys. Rev. D **105**, 074511 (2022).

[15] P. de Forcrand and O. Philipsen, The QCD phase diagram for small densities from imaginary chemical potential, Nucl. Phys. **B642**, 290 (2002).

[16] M. D'Elia and M.-P. Lombardo, Finite density QCD via imaginary chemical potential, Phys. Rev. D **67**, 014505 (2003).

[17] M. D'Elia, F. Di Renzo, and M. P. Lombardo, The strongly interacting quark gluon plasma, and the critical behaviour of QCD at imaginary mu, Phys. Rev. D **76**, 114509 (2007).

[18] P. Cea, L. Cosmai, M. D'Elia, C. Manneschi, and A. Papa, Analytic continuation of the critical line: Suggestions for QCD, Phys. Rev. D **80**, 034501 (2009).
[19] C. Bonati, M. D'Elia, M. Mariti, M. Mesiti, F. Negro, and F. Sanfilippo, Curvature of the chiral pseudocritical line in QCD: Continuum extrapolated results, Phys. Rev. D **92**, 054503 (2015).
[20] P. Cea, L. Cosmai, and A. Papa, Critical line of $2+1$ flavor QCD: Toward the continuum limit, Phys. Rev. D **93**, 014507 (2016).
[21] R. Bellwied, S. Borsanyi, Z. Fodor, J. Guenther, S. D. Katz, C. Ratti, and K. K. Szabo, The QCD phase diagram from analytic continuation, Phys. Lett. B **751**, 559 (2015).
[22] V. Vovchenko, A. Pasztor, Z. Fodor, S. D. Katz, and H. Stoecker, Repulsive baryonic interactions and lattice QCD observables at imaginary chemical potential, Phys. Lett. B **775**, 71 (2017).
[23] V. Vovchenko, J. Steinheimer, O. Philipsen, and H. Stoecker, Cluster expansion model for QCD baryon number fluctuations: No phase transition at $\mu_B/T < \pi$, Phys. Rev. D **97**, 114030 (2018).
[24] S. Borsányi, Z. Fodor, J. N. Guenther, R. Kara, S. D. Katz, P. Parotto, A. Pásztor, C. Ratti, and K. K. Szabó, Lattice QCD equation of state at finite chemical potential from an alternative expansion scheme, Phys. Rev. Lett. **126**, 232001 (2021).
[25] S. Borsanyi, J. N. Guenther, R. Kara, Z. Fodor, P. Parotto, A. Pasztor, C. Ratti, and K. K. Szabo, Resummed lattice QCD equation of state at finite baryon density: Strangeness neutrality and beyond, Phys. Rev. D **105**, 114504 (2022).
[26] I. M. Barbour, S. E. Morrison, E. G. Klepfish, J. B. Kogut, and M.-P. Lombardo, Results on finite density QCD, Nucl. Phys. B, Proc. Suppl. **60**, 220 (1998).
[27] Z. Fodor and S. D. Katz, A new method to study lattice QCD at finite temperature and chemical potential, Phys. Lett. B **534**, 87 (2002).
[28] Z. Fodor and S. D. Katz, Lattice determination of the critical point of QCD at finite T and mu, J. High Energy Phys. 03 (2002) 014.
[29] Z. Fodor and S. D. Katz, Critical point of QCD at finite T and mu, lattice results for physical quark masses, J. High Energy Phys. 04 (2004) 050.
[30] P. de Forcrand, S. Kim, and T. Takaishi, QCD simulations at small chemical potential, Nucl. Phys. B, Proc. Suppl. **119**, 541 (2003).
[31] A. Alexandru, M. Faber, I. Horvath, and K.-F. Liu, Lattice QCD at finite density via a new canonical approach, Phys. Rev. D **72**, 114513 (2005).
[32] Z. Fodor, S. D. Katz, and C. Schmidt, The density of states method at non-zero chemical potential, J. High Energy Phys. 03 (2007) 121.
[33] G. Endrodi, Z. Fodor, S. D. Katz, D. Sexty, K. K. Szabo, and C. Torok, Applying constrained simulations for low temperature lattice QCD at finite baryon chemical potential, Phys. Rev. D **98**, 074508 (2018).
[34] M. Giordano, K. Kapas, S. D. Katz, D. Nogradi, and A. Pasztor, Effect of stout smearing on the phase diagram from multiparameter reweighting in lattice QCD, Phys. Rev. D **102**, 034503 (2020).
[35] M. Giordano, K. Kapas, S. D. Katz, D. Nogradi, and A. Pasztor, New approach to lattice QCD at finite density; Results for the critical end point on coarse lattices, J. High Energy Phys. 05 (2020) 088.
[36] S. Borsanyi, Z. Fodor, M. Giordano, S. D. Katz, D. Nogradi, A. Pasztor, and C. H. Wong, Lattice simulations of the QCD chiral transition at real baryon density, Phys. Rev. D **105**, L051506 (2022).
[37] S. Borsanyi, Z. Fodor, M. Giordano, J. N. Guenther, S. D. Katz, A. Pasztor, and C. H. Wong, Equation of state of a hot-and-dense quark gluon plasma: Lattice simulations at real μB vs extrapolations, Phys. Rev. D **107**, L091503 (2023).
[38] G. Basar, QCD critical point, Lee-Yang edge singularities, and Padé resummations, Phys. Rev. C **110**, 015203 (2024).
[39] D. A. Clarke, P. Dimopoulos, F. Di Renzo, J. Goswami, C. Schmidt, S. Singh, and K. Zambello, Searching for the QCD critical endpoint using multi-point Padé approximations, Phys. Rev. D **112**, L091504 (2025).
[40] A. Adam, S. Borsányi, Z. Fodor, J. N. Guenther, P. Parotto, A. Pásztor, D. Pesznyák, L. Pirelli, and C. H. Wong, Search for a Lee-Yang edge singularity in high-statistics Wuppertal-Budapest data, Proc. Sci. LATTICE2024 (**2025**) 178 [arXiv:2502.03211].
[41] J. Adam *et al.* (STAR Collaboration), Nonmonotonic energy dependence of net-proton number fluctuations, Phys. Rev. Lett. **126**, 092301 (2021).
[42] M. Abdallah *et al.* (STAR Collaboration), Cumulants and correlation functions of net-proton, proton, and antiproton multiplicity distributions in Au $+$ Au collisions at energies available at the BNL Relativistic Heavy Ion Collider, Phys. Rev. C **104**, 024902 (2021).
[43] B. E. Aboona *et al.*, Precision Measurement of Net-Proton-Number Fluctuations in Au+Au Collisions at RHIC, Phys. Rev. Lett. **135**, 142301 (2025).
[44] P. Braun-Munzinger, B. Friman, K. Redlich, A. Rustamov, and J. Stachel, Relativistic nuclear collisions: Establishing the non-critical baseline for fluctuation measurements, Nucl. Phys. **A1008**, 122141 (2021).
[45] V. Vovchenko, V. Koch, and C. Shen, Proton number cumulants and correlation functions in Au-Au collisions at sNN=7.7–200 GeV from hydrodynamics, Phys. Rev. C **105**, 014904 (2022).
[46] P. Isserstedt, M. Buballa, C. S. Fischer, and P. J. Gunkel, Baryon number fluctuations in the QCD phase diagram from Dyson-Schwinger equations, Phys. Rev. D **100**, 074011 (2019).
[47] W.-j. Fu, J. M. Pawlowski, and F. Rennecke, QCD phase structure at finite temperature and density, Phys. Rev. D **101**, 054032 (2020).
[48] F. Gao and J. M. Pawlowski, Chiral phase structure and critical end point in QCD, Phys. Lett. B **820**, 136584 (2021).
[49] F. Gao and J. M. Pawlowski, QCD phase structure from functional methods, Phys. Rev. D **102**, 034027 (2020).
[50] P. J. Gunkel and C. S. Fischer, Locating the critical endpoint of QCD: Mesonic backcoupling effects, Phys. Rev. D **104**, 054022 (2021).
[51] W.-j. Fu, X. Luo, J. M. Pawlowski, F. Rennecke, R. Wen, and S. Yin, Hyper-order baryon number fluctuations at finite temperature and density, Phys. Rev. D **104**, 094047 (2021).

[52] R. Critelli, J. Noronha, J. Noronha-Hostler, I. Portillo, C. Ratti, and R. Rougemont, Critical point in the phase diagram of primordial quark-gluon matter from black hole physics, Phys. Rev. D **96**, 096026 (2017).

[53] M. Hippert, J. Grefa, T. A. Manning, J. Noronha, J. Noronha-Hostler, I. Portillo Vazquez, C. Ratti, R. Rougemont, and M. Trujillo, Bayesian location of the QCD critical point from a holographic perspective, Phys. Rev. D **110**, 094006 (2024).

[54] L. Zhu, X. Chen, K. Zhou, H. Zhang, and M. Huang, Bayesian inference of the critical endpoint in $2+1$-flavor system from holographic QCD, Phys. Rev. D **112**, 026019 (2025).

[55] E. S. Fraga, L. F. Palhares, and P. Sorensen, Finite-size scaling as a tool in the search for the QCD critical point in heavy ion data, Phys. Rev. C **84**, 011903 (2011).

[56] R. A. Lacey, Indications for a critical point in the phase diagram for hot and dense nuclear matter, Nucl. Phys. **A956**, 348 (2016).

[57] A. Sorensen and P. Sorensen, Locating the critical point for the hadron to quark-gluon plasma phase transition from finite-size scaling of proton cumulants in heavy-ion collisions, arXiv:2405.10278.

[58] J. Steinheimer, M. Omana Kuttan, T. Reichert, Y. Nara, and M. Bleicher, Predicting the QCD critical point and EoS from combining HIC and neutron star observations, Phys. Lett. B **867**, 139605 (2025).

[59] H. Shah, M. Hippert, J. Noronha, C. Ratti, and V. Vovchenko, Locating the QCD critical point from first principles through contours of constant entropy density, arXiv:2410.16206.

[60] S. Borsanyi, Z. Fodor, C. Hoelbling, S. D. Katz, S. Krieg, and K. K. Szabo, Full result for the QCD equation of state with $2+1$ flavors, Phys. Lett. B **730**, 99 (2014).

[61] S. Borsányi, Z. Fodor, J. N. Guenther, R. Kara, P. Parotto, A. Pásztor, L. Pirelli, and C. H. Wong, Chiral versus deconfinement properties of the QCD crossover: Differences in the volume and chemical potential dependence from the lattice, Phys. Rev. D **111**, 014506 (2025).

[62] See Supplemental Material at http://link.aps.org/supplemental/10.1103/rj6r-dmg9 for further details on the analysis.

[63] L. Adamczyk *et al.* (STAR Collaboration), Bulk properties of the medium produced in relativistic heavy-ion collisions from the beam energy scan program, Phys. Rev. C **96**, 044904 (2017).

[64] A. Andronic, P. Braun-Munzinger, K. Redlich, and J. Stachel, Decoding the phase structure of QCD via particle production at high energy, Nature (London) **561**, 321 (2018).

[65] A. Lysenko, M. I. Gorenstein, R. Poberezhniuk, and V. Vovchenko, Chemical freeze-out curve in heavy-ion collisions and the QCD critical point, Phys. Rev. C **111**, 054903 (2025).

[66] S. Borsanyi *et al.*, Calculation of the axion mass based on high-temperature lattice quantum chromodynamics, Nature (London) **539**, 69 (2016).

[67] S. Borsanyi, Z. Fodor, J. N. Guenther, P. Parotto, A. Pasztor, L. Pirelli, K. K. Szabo, and C. H. Wong, QCD deconfinement transition line up to $\mu B = 400$ MeV from finite volume lattice simulations, Phys. Rev. D **110**, 114507 (2024).

[68] J. Engels, J. Fingberg, F. Karsch, D. Miller, and M. Weber, Nonperturbative thermodynamics of SU(N) gauge theories, Phys. Lett. B **252**, 625 (1990).

[69] R. Bellwied, S. Borsanyi, Z. Fodor, S. D. Katz, A. Pasztor, C. Ratti, and K. K. Szabo, Fluctuations and correlations in high temperature QCD, Phys. Rev. D **92**, 114505 (2015).

[70] S. Borsanyi, G. Endrodi, Z. Fodor, A. Jakovac, S. D. Katz, S. Krieg, C. Ratti, and K. K. Szabo, The QCD equation of state with dynamical quarks, J. High Energy Phys. 11 (2010) 077.

[71] S. Borsanyi *et al.*, Leading hadronic contribution to the muon magnetic moment from lattice QCD, Nature (London) **593**, 51 (2021).

[72] A. M. Halasz, A. D. Jackson, R. E. Shrock, M. A. Stephanov, and J. J. M. Verbaarschot, On the phase diagram of QCD, Phys. Rev. D **58**, 096007 (1998).

[73] H. T. Ding *et al.* (HotQCD Collaboration), Chiral phase transition temperature in $(2+1)$-flavor QCD, Phys. Rev. Lett. **123**, 062002 (2019).

[74] A. Y. Kotov, M. P. Lombardo, and A. Trunin, QCD transition at the physical point, and its scaling window from twisted mass Wilson fermions, Phys. Lett. B **823**, 136749 (2021).

[75] www.gauss-centre.eu.

[76] Wuppertal Budapest Collaboration, Continuum extrapolated equation of state at zero density, 10.5281/zenodo.17793649 (2025).